Applied Catalysis B: Environmental 150–151 (2014) 506–514

Contents lists available at ScienceDirect

Applied Catalysis B: Environmental

journal homepage: www.elsevier.com/locate/apcatb

Low CO generation on tunable oxygen vacancies of non-precious metallic Cu/ZnO catalysts for partial oxidation of methanol reaction

Kuan-Yi Lee, Yuh-Jeen Huang*

Department of Biomedical Engineering and Environmental Sciences, National Tsing Hua University, Hsinchu, 30013 Taiwan, ROC

ARTICLE INFO

Article history:
Received 30 August 2013
Received in revised form
16 December 2013
Accepted 23 December 2013
Available online 31 December 2013

Keywords:
Partial oxidation of methanol (POM)
Oxygen vacancies
Non-precious metallic CuZn-based catalyst
CO-free

ABSTRACT

A simple and inexpensive method is proposed to modulate oxygen vacancies on the non-precious metallic CuZn-based catalyst surface. The identification and quantification of these oxygen vacancies on vZ (ZnO containing oxygen vacancies) and the catalytic activities of CvZ (Cu on ZnO containing oxygen vacancies, ca. 30 wt.% Cu and 70 wt.% Zn) during partial oxidation of methanol (POM) reaction are discussed. The vZ was calcined in a nitrogen atmosphere at various temperatures (450 °C, 500 °C and 550 °C), and catalytic activities of CvZ catalysts prepared in deposition precipitation (DP) and co-precipitation (CP) and CZr (Cu on ZrO_2, ca. 30 wt.% Cu and 70 wt.% Zr) catalysts were performed. The efficiency of both CP-CvZ-450 and DP-CvZ-450 catalysts are excellent with 100% of C_{MeOH} and 95% of F_{H_2} at 250 °C, and 70% of C_{MeOH} and >75% F_{H_2} at 150 °C. Significantly, F_{CO} was kept at 0–4% at $T < 250$ °C with better stability for DP-CvZ-450 catalyst, as well. Moreover, a CO-free situation could be achieved for both DP-CvZ-500 and DP-CvZ-550 which contain more oxygen vacancies. These oxygen vacancies on the surface: enhanced an affinity for adsorbing reactant oxygen atoms; induced decomposition of intermediates species, and; can even catalyze CO oxidation at a lower temperature.

1. Introduction

Energy used for transportation, high technology, manufacturing and many other industries is very important in the daily life of modern societies. Several alternative energies, particularly hydrogen energy, have been extensively developed during the last few decades. One of methanol reforming reactions, catalytic partial oxidation of methanol (POM) [1–3], which is an exothermic reaction with many advantages including higher reaction rates without the need for an additional heat supply, especially if the reaction reaches a steady-state, is applied in the methanol reformer as a hydrogen-rich gas supplier in the fuel-cell system.

Recently, Cu-based catalysts having high activity, good selectivity, low cost, environmental friendliness, and natural abundance, have been widely investigated in several reactions, such as: methanol synthesis, water–gas shift (WGS) reaction, preferential oxidation, and methanol reforming, etc. [4–6]. Copper supported with zinc oxide provides high conversion, high H_2 selectivity in POM reaction [7–11]. Some researchers have compared the influences of different copper loadings over Cu/ZnO (CZ) catalysts and have indicated catalytic activity was increased by a higher surface area of metallic copper [12]. However, there are several disadvantages of copper catalysts, such as high CO concentration, high ignition temperature, poor structural stability, and short lifetime.

ZnO, the support for our catalyst, has been most frequently studied because of its numerous applications, such as photocatalysis, light-emitting materials, solar energy conversion, and chemical sensors [13–17]. Generally, in the aromatization of light alkane catalysis, ZnO plays the role of removing hydrogen species encamped at the acid site of zeolites [18]. In addition, in methanol reforming, such as methanol decomposition (MD), stream reforming of methanol (SRM), or POM reaction over CZ based catalyst, ZnO also promotes desorption of hydrogen, and simultaneously raising hydrogen selectivity [19,20]. According to the above studies of POM, some authors [21,22] used precious metals, such as Au, to reduce CO by-product and lower the reaction temperature. Price should be considered in such circumstances, however. Doping with transition metals [23,24], such as Zr and Ce, would generate native defects (oxygen vacancies), but sometimes the overall catalytic activity would be sacrificed. Nano-structure ZnO also has been used in catalytic methanol-synthesis reaction, causing the presence of a polar ZnO (000$\bar{1}$) surface upon which oxygen vacancies have formed on the surface of crystals serving as the active site [25,26]. ZnO, within oxygen vacancies on the lattice, could absorb CO or CO_2 during the initiation of methanol synthesis. Lin et al. [27] used the CuO–ZnO inverse opals to generate oxygen vacancies by O_2-plasma treatment and promote greater methanol microreformer efficiency; but the process for preparing catalysts used by Lin et al.

* Corresponding author. Department of Biomedical Engineering and Environmental Sciences, National Tsing Hua University, Hsinchu, Taiwan 30013, ROC.
Tel.: +886 35715131x35496; fax: +886 35718649.
E-mail address: yjhuang@mx.nthu.edu.tw (Y.-J. Huang).

0926-3373/$ – see front matter © 2013 Elsevier B.V. All rights reserved.
http://dx.doi.org/10.1016/j.apcatb.2013.12.044

is not commonly utilized. In this study, we propose a new, simple and inexpensive method to modulate oxygen vacancies on the surface of the non-precious metallic CZ catalyst and hope these oxygen vacancies can lower the CO by-product and improve catalytic activities in the POM reaction. The important factors for oxygen vacancies generation, such as calcined temperature, preparation methods [co-precipitation (CP) and deposition precipitation (DP)], and the influence of oxygen vacancies on catalytic performance for POM reaction, are discussed in detail. Moreover, a ZrO_2 support containing an oxygen-vacancy structure was used to compare the effects of different materials.

2. Experimental

2.1. Catalyst preparation

The synthesis of ZnO nanoparticles (NPs), which are the support of our catalysts, was first prepared via a simple chemical precipitation method [14,28]. Stoichiometric $ZnCl_2$ (0.25 M) and sodium dodecyl sulfate (SDS, 0.00025 M) were introduced into 100 mL of deionized water. Then NH_4HCO_3 (0.5 M) solution was poured slowly in and mixed well under constant magnetic stirring. After 2 h of reaction, the precipitates were filtered and washed thoroughly with 800 mL of anhydrous ethanol to remove impurities, and then dried in a vacuum oven at 60 °C overnight. Finally, a general ZnO NPs with no oxygen vacancies was calcined in air at 450 °C. For ZnO NPs with oxygen vacancies, the catalysts were calcined in N_2 (~99.99%) at 450 °C, 500 °C, or 550 °C, respectively, for 1.5 h and then calcined in air at 450 °C for 0.5 h to yield fresh ZnO NPs (designated as vZ-450, vZ-500, and vZ-550).

A series of Cu/v-ZnO catalysts which contained oxygen vacancies on the ZnO (designated as DP-CvZ-450, DP-CvZ-500, and DP-CvZ-550) was prepared by DP method. ZnO NPs with oxygen vacancies were first dispersed in 500 mL of deionized water with vigorous stirring at 70 °C. An appropriate portion of copper nitrate solution was added to the above-mentioned solution and Na_2CO_3 solution was used to maintain the mixture at pH = 7. After aging to pH = 8, the precipitates were filtrated and washed thoroughly with deionized water, and then dried at 105 °C overnight. The catalysts were calcined in N_2 at 450 °C for 1.5 h and then in air for 0.5 h to remove impurities.

Copper-based catalysts CZ (30 wt.% Cu and 70 wt.% Zn) and Cu/ZrO_2 (CZr) (30 wt.% Cu and 70 wt.% Zr) were prepared by CP of metal nitrates in aqueous solution. This method is based on our previous study [21,29]. Another CZ (CP-CvZ-450) with oxygen vacancies on the ZnO surface was prepared by CP of metal chlorides in aqueous solution. In short, $CuCl_2$ and $ZnCl_2$ solutions (0.5 M) were added to 500 mL of deionized water at 70 °C. The required portion of 2 M Na_2CO_3 solution was quickly added while energetically stirring the solution. After aging to pH = 8, the precipitates were filtrated and residue was washed thoroughly with deionized water, and then dried overnight at 105 °C. The final catalysts were calcined in N_2 at 450 °C for 1.5 h and then calcined in air for 0.5 h to remove impurities. All catalysts are summarized in Table 1.

2.2. Characterization

The exact compositions of the catalysts were analyzed by ICP-MS (Perkin–Elmer, SCIEX ELAN 5000). Each catalyst's compositions are summarized in Table 2.

X-ray powder diffraction (XRD) patterns were obtained by Rigaku TTRAX III equipped with an 18 KW rotating anode Cu target (λ = 0.15406 nm). The patterns were obtained from 20 to 80° at a rate of 4 °C min^{-1}.

Table 1
A summary of the catalysts and their prepared conditions.

Catalyst	Preparation method	Calcine conditions	
		N_2	Air
Z[a]	Precipitation	-	450 °C, 2 h
vZ[b]-450	Precipitation	450 °C, 1.5 h	450 °C, 0.5 h
vZ-500	Precipitation	500 °C, 1.5 h	450 °C, 0.5 h
vZ-550	Precipitation	550 °C, 1.5 h	450 °C, 0.5 h
DP-CvZ[c]-450	Deposition precipitation	450 °C, 1.5 h	450 °C, 0.5 h
DP-CvZ-500	Deposition precipitation	450 °C, 1.5 h	450 °C, 0.5 h
DP-CvZ-550	Deposition precipitation	450 °C, 1.5 h	450 °C, 0.5 h
CP-CvZ-450	Co-precipitation	450 °C, 1.5 h	450 °C, 0.5 h
CZ[d]	Co-precipitation	-	400 °C, 4 h
CZr[e]	Co-precipitation	-	400 °C, 4 h

[a] ZnO nano-particles.
[b] ZnO with oxygen vacancies.
[c] Cu/ZnO with oxygen vacancies.
[d] Cu/ZnO catalyst.
[e] Cu/ZrO_2 catalyst.

X-ray photoelectron spectroscopy (XPS) to study the chemical shift and oxidation state of the catalyst surface was obtained by ESCA PHI 1600 spectrometer with Al/Mg dual anode X-ray sources (1486.6 and 1253.6 eV, respectively). For experiments, the O1s, Zn2p3 core-level spectra were recorded and the corresponding binding energies were referenced to the C1s line at 284.9 eV [8].

For photoluminescence (PL) experiments, powder samples were spindled first, then fixed onto the sample holder. The device, a 325 nm laser line from He–Cd Laser was utilized for excitation, and the scan range was set between 300 and 700 nm. The laser was cut by optical chopper (Ω_m), then focused on the sample by convex lens. The fluorescent light beam which radiated from the sample entered the spectrometer from the convex lens, and was received by a detector after grating. The frequency of Ω_m was the signal of fluorescence spectroscopy.

The micro-Raman spectra, were recorded at room temperature in a confocal microscope (Jobin Yvon, MFO) combined with a monochromator system (Jobin Yvon, iHR550) and a liquid-nitrogen-cooled, charge-coupled device camera (Jobin Yvon, 1024 × 256 pixels). As an excitation source we used the 514.5 nm line of argon laser (Modu-Laser, Stellar-Pro 514/50).

For the temperature-programmed reduction (TPR) and temperature-programmed desorption of oxygen (O_2-TPD) tests, a system equipped with gold-coated TCD and Brooks 5850E mass flow controller was used. Approximate 55 mg of each fresh catalyst was placed into a U-shaped quartz. In each TPR run, a sample of 55 mg in a U-shape tube reactor of 4 mm inner diameter (i.d.) was reduced by 10% H_2/N_2 or 10% CO/He for H_2-TPR or CO-TPR, respectively, at a flow rate of 30 mL/min upon raising the temperature of the sample from room temperature to 500 °C with a heating ramp up of 7 °C min^{-1}. The software used for peak integration was provided by Scientific Information Service Corporation (SISC). For O_2-TPD test, 55 mg of sample were preheated at 450 °C for 2 h in flowing He (purity: 99.9995%) to desorb adsorbed gases on the surface and then cooled down to room temperature. Next, the catalyst was treated in O_2 (purity: 99.999%) at 200 °C for 1 h and then cooled in flowing O_2 to room temperature. The gas mixture was switched to He to flush the reactor for 1 h to remove gas-phase O_2 completely. Then, the O_2 adsorption procedure was repeated one more time to ensure the saturation with O_2 chemisorption. Subsequently, the O_2 desorption experiment was carried out by ramping the temperature up from 7 °C min^{-1} to 450 °C.

The POM reaction gas (methanol and oxygen) chemisorption at various temperatures (ambient, 160, 180, 200, and 300 °C) on the surface of catalysts was done by infrared spectroscopy (Thermo Scientific NICOLET 6700) with a diffuse reflectance infrared Fourier transform spectra (DRIFTS) accessory (Harrick) and a MCT/A

Table 2
Physical properties of freshly CZ catalysts.

Catalyst	C_{ov}[a]	Metallic loading (wt. %)[b]			Particle size (nm)[c]		
		Cu (%)	Zn (%)	Zr (%)	$d_{ZnO(101)}$	$d_{ZrO_2(101)}$	$d_{CuO(111)}$
Z	0.08	0	100	0	18.9	-	-
vZ-450	6.53	0	100	0	19.1	-	-
vZ-500	8.32	0	100	0	20.7	-	-
vZ-550	11.63	0	100	0	23.1	-	-
DP-CvZ-450	2.26	29.5	70.5	0	22.4	-	13.4
DP-CvZ-500	2.69	30.4	69.6	0	23.7	-	13.4
DP-CvZ-550	6.97	30.2	69.8	0	25.7	-	13.7
CP-CvZ-450	1.84	30.0	70.0	0	6.9	-	5.2
CZ	0.09	29.2	70.8	0	10.8	-	6.7
CZr	1.23	34.5	0	65.5	-	Amorphous	Amorphous

[a] The concentration of oxygen vacancies (C_{ov}) which calculated by PL spectra (V_o = intensity$_{523}$/intensity$_{377}$, each sample was normalized at peaks of 377 nm).
[b] Chemical analysis result from ICP-MS.
[c] Normal diameter estimated from XRD data using the Debye–Scherrer equation.

detector. About 1.0 g of the catalyst was packed in the sample holder of the in-situ cell, subsequently heated by a thermostatically controlled process and pretreated at 300 °C for 30 min in a flow of nitrogen (>99.99%) to remove water and carbonate on the catalyst surface. After feeding reaction gases (CH_3OH and O_2/Ar), with an O_2/CH_3OH ratio of 0.5 for 10 min at chemisorption temperature, samples were purged by nitrogen (>99.99%) for 10 min to remove reversibly adsorbed species. The spectra were collected at a resolution of 4 cm^{-1} and an accumulation of 32 scans. The CO chemisorption experiments were similarly performed. The CO gas (1% with 99% Ar) was used and the spectra were collected at an accumulation of 128 scans.

2.3. Catalytic test

Catalytic activity measurements were conducted in a fixed bed reactor (4 mm i.d.) operating at atmospheric pressure. Freshly calcined catalysts were pulverized into fine powders, pressed into disks, crushed and sieved through 60–80 mesh for POM. The methanol was fed to the evaporator by means of a piston pump, and the gases—Ar, O_2—were fed by a Brooks 5850E mass flow controller. The molar ratio of oxygen to methanol (O/M) was controlled at 0.5. The gas hourly space velocity (GHSV) and weight hourly space velocity (WHSV) were controlled at 60,000 h^{-1} and 9.48 h^{-1}, respectively, and the performance of the reactions over catalysts was measured at 250, 225, 200, 175, and 150 °C, respectively. Reaction products were analyzed by a GC-TCD equipped with columns, Porapak Q (H_2, CO_2, and CO) and Molecular Sieve 5A (CO_2, H_2O, and CH_3OH) in parallel. H_2, CO_2, CO, H_2O were found in the reforming reactions. Methanol conversion (C_{MeOH}), fraction of hydrogen in methanol being converted to H_2 (F_{H_2}), and fraction of carbon in methanol being converted to CO (F_{CO}) are generally defined as:

$$C_{MeOH}(\%) = \frac{\left(n_{MeOH,in} - n_{MeOH,out}\right)}{n_{MeOH,in}} \times 100\% \quad (2\text{-}1)$$

$$F_{H_2} = \frac{1\, n_{H_2}}{2\left(n_{MeOH,in} - n_{MeOH,out}\right)} \times 100\% \quad (2\text{-}2)$$

$$F_{CO} = \frac{n_{CO}}{\left(n_{MeOH,in} - n_{MeOH,out}\right)} \times 100\% \quad (2\text{-}3)$$

3. Results and discussion

3.1. Synthesis of tunable oxygen vacancies on ZnO

The ZnO NPs as support usually used in catalytic hydrogen generation can be prepared by chemical precipitation method under various conditions. Different calcination atmospheres and temperatures might affect the structure and properties of ZnO NPs [14]. Comparing the different XRD patterns of ZnO NPs with various calcined temperatures, Fig. 1 (a)–(d) shows only hexagonal wurtzite ZnO peaks, and no excess impurities peaks were observed for each ZnO NPs. The size of ZnO NPs samples, derived by estimating a ZnO(101) peak of 36.3°, through the Debye–Scherer formula, are displayed in Table 2 and are approximately 18.9, 19.1, 20.7, 23.1 nm, respectively. This clearly reveals that the particle size of ZnO NPs (b–d) increased with increasing temperature.

To confirm that the variations in structure and properties were due to the formation of oxygen vacancies on the ZnO surface via different calcined conditions, the PL spectra [Fig. 2 (I)] which produced "green" luminescence at $\lambda \sim 525$ nm by defects (oxygen vacancy, zinc vacancy, interstitial zinc, interstitial oxygen, or antisite oxygen, etc.) in the ZnO lattices [30–32] was studied. Dai et al. [33] also suggested that the intense green emission is associated with the concentration of singly ionized oxygen vacancies. Fig. 2 (I) obviously shows that the peaks of the green emission were increased with increasing calcination temperature. Moreover, in order to evaluate the concentration of oxygen vacancies (C_{ov}) on ZnO, the peak near $\lambda = 377$ nm attributed to the recombination of free excitons through an exciton–exciton collision process [34], was normalized for each sample first. Then, the C_{ov} were calculated from the ratio of peak $\lambda = 377$ nm and peak $\lambda = 525$ nm [see Fig. 2 (I) and Table 2]. Of particular noteworthiness, the value of vZ-550 reaches maximum, demonstrating that it has the highest concentration of oxygen vacancies. Furthermore, similar results showing in XPS experiments (Table 3) revealed that the percentage of surface

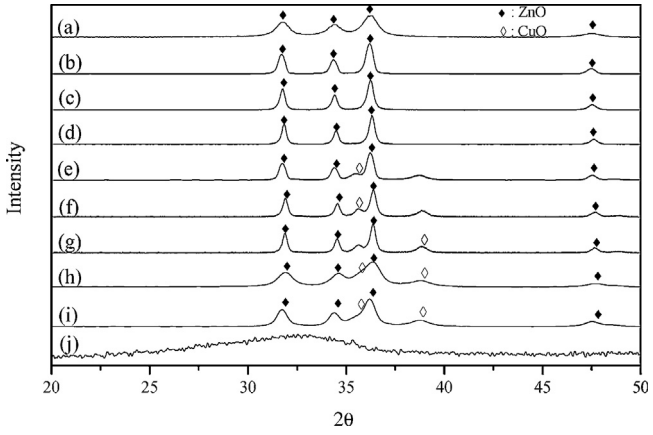

Fig. 1. XRD patterns of (a) Z, (b) vZ-450, (c) vZ-500, (d) vZ-550, (e) DP-CvZ-450, (f) DP-CvZ-500, (g) DP-CvZ-550, (h) CP-CvZ-450, (i) CZ, and (j) CZr catalysts.

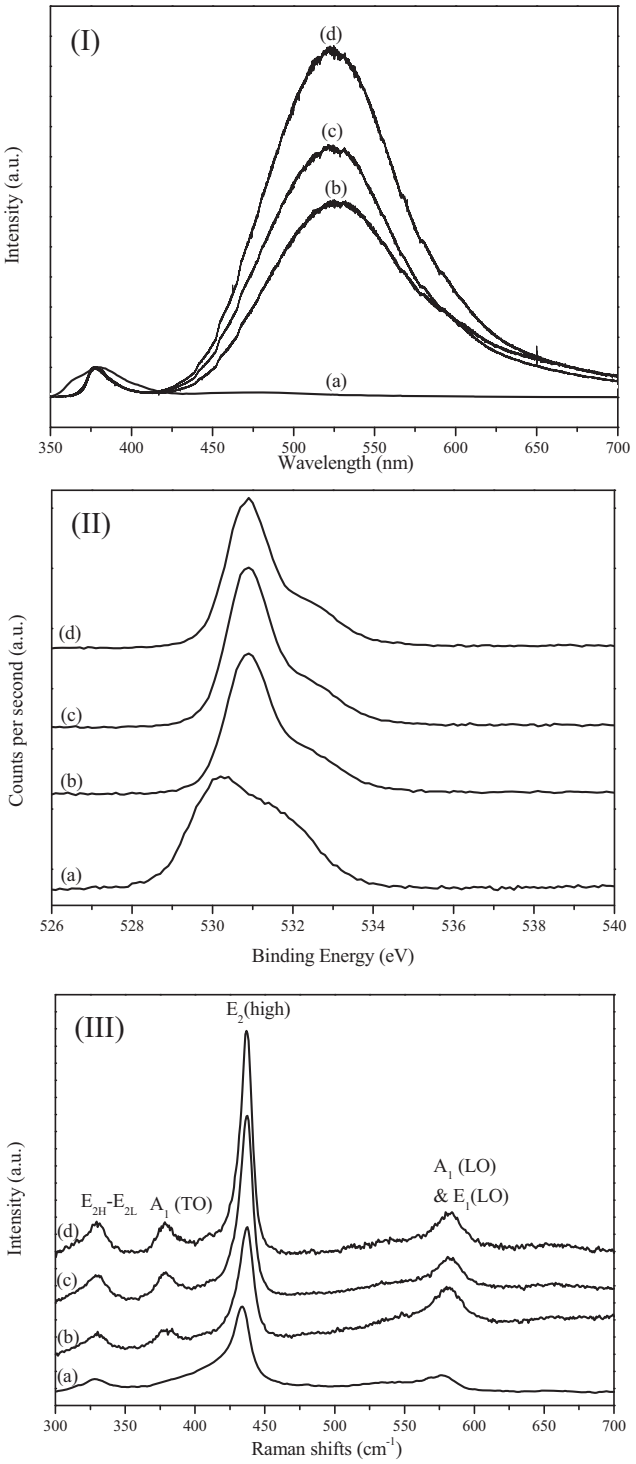

Fig. 2. The material identification of oxygen vacancies via (I) PL spectra, (II) XPS spectra of O1s, and (III) Micro-Raman spectra over ZnO NPs samples (a) Z, (b) vZ-450, (c) vZ-500, and (d) vZ-550.

oxygen obviously decreased from 58.5% of Z to around 37% of vZ samples, and vZ-450 (36.7%) has the lowest surface oxygen percentage of overall samples. The O1s core level spectra of Z in Fig. 2 (II)-(a) display the main peak around 529–531 eV which is typically attributed to oxygen ions in the ZnO lattices, but for that of vZ-450, vZ-500, and vZ-550 (curve b–d) the main peak at around 530–532 eV slightly shifted to a higher binding energy. This is normally contributed to by oxygen-deficiency on the surface [35–38]. Despite more oxygen-deficiency on the vZ-500 or vZ-550 measured

Table 3
The atomic concentration and oxygen vacancies concentration ratio for ZnO catalysts.

Catalyst	Atomic concentration on surface[a]	
	O1s	Zn2p3
Z	58.54%	41.46%
vZ-450	36.70%	63.30%
vZ-500	37.61%	62.39%
vZ-550	38.00%	62.00%

[a] Calculate via XPS experiments.

from the PL, oxygen migrating rapidly to surface at 500 °C or 550 °C might cause higher oxygen ratios than on vZ-450 [32] (see Table 3).

To further discuss the effect of annealing temperature in the presence of oxygen vacancies, Raman spectra [Fig. 2 (III)] was investigated and described as follows. From the spectra, the peak appearing at around 436 cm^{-1} could be assigned to E_2 (high) modes of a typical wurtzite hexagonal phase of ZnO, and the peak at around 578 cm^{-1} due to superimposition of A_1 (LO) and E_1 (LO) was attributed to oxygen vacancies on the ZnO [14,27]. Compared with Z (curve a), another A_1 (TO) mode which reflects the strength of the polar lattice bonds appeared at around 379 cm^{-1} for four vZ samples (curve b–d) [39]. In addition, vZ-500 and vZ-550 clearly have the strong peak of E2 (high) mode because they had very good crystalline quality. These results are observably confirmed by XRD. However, the E2 (high) mode of vZ-450 was broad; presumably the band structure of ZnO was more disordered.

3.2. The effect of prepared methods of CZ

In this study, two methods were used to prepare CZ catalysts which have oxygen vacancies on the surface. First, DP method was used to load Cu on aforementioned ZnO NPs. For the resulting XRD pattern (Fig. 1) and particle size (Table 2), particle size grew slightly after the second calcination, and a hard-to-distinguish peak at around 36°, with another peak at 38.8° attributed to the discovery of small CuO particles. The CuO particle size was approximately 13–14 nm of all DP-CvZ samples. The DP-CvZ samples of C_{ov} (Table 2) decreased a little after Cu loading, hence those oxygen vacancies would reduce through the second calcination, or the CuO could restrain the ZnO from emitting green luminescence. However, the DP-CvZ-550 catalyst still maintained the maximum C_{ov} value at 6.97.

Another way to prepare CZ with an oxygen-vacancy catalyst is the CP method (CP-CvZ-450). By this method, CP-CvZ-450 catalyst can obtain the most minimal particle size for both ZnO and CuO, approximately 6.9 and 5.2 nm, respectively. To compare further with DP-CvZ-450, CP-CvZ-450 catalyst has the lower C_{ov} value at 1.84 due to poor circumstances for oxygen vacancies to generate on ZnO. At the same time, poor crystallinity was obtained by CP method. Some papers [10,40,41] also indicate more amorphous phases and smaller particles by CP.

3.3. Hydrogen TPR

The temperature profile of the TPR pattern of CZ-based catalysts w/wo oxygen vacancies are shown in Fig. 3. From the profiles, the CZ (curve e) displays a main peak at $T \sim 205$ °C, with a front shoulder at around 190 °C, which is associated with reduced interaction with the support of CuO species; even so, the CP-CvZ-450 (curve d) shows an analogical reduction curve, while the front shoulder becomes more distinct. The reduction temperature of CuO species in contact with ZnO was lower than isolated CuO [42]. There were similar results in our previous study [29]; thus, we suggest that the front shoulder and main peak reveal ZnO-assisted reduction of CuO,

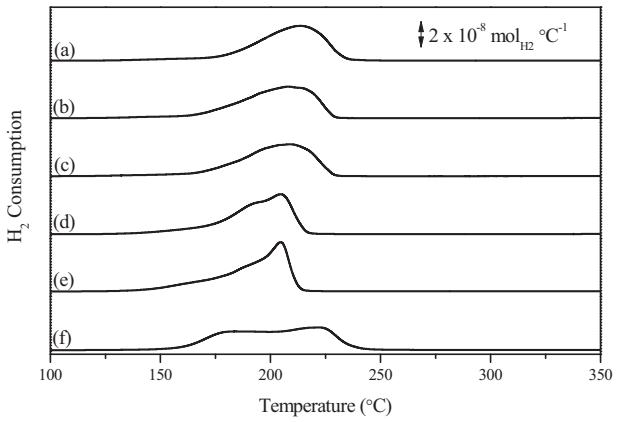

Fig. 3. The H_2-TPR profiles of freshly catalysts (a) DP-CvZ-450, (b) DP-CvZ-500, (c) DP-CvZ-550, (d) CP-CvZ-450, (e) CZ, and (f) CZr.

which took place in a stepwise fashion. Nevertheless, interestingly, the series of DP-CvZ catalysts (curve a–c) has a broad peak of around 180–230 °C, showing a similar bonding to ZnO and an identical CuO particle size as observed by XRD analysis (Table 2). Accordingly, despite containing oxygen vacancies (DP-CvZ-450, DP-CvZ-500, DP-CvZ-550, and CP-CvZ-450), it seems that they would form a Cu–Zn complex that could enhance reducibility.

Moreover, another catalyst, CZr, using ZrO_2 as support, has been extensively studied for the advantages of a monoclinic ZrO_2 phase which has a relatively higher population of oxygen vacancies [43,44]. The CZr catalyst (curve f) has peaks distinct from CZ-based catalysts. The front shoulder is located at around 175 °C which could also be attributed to the strong interaction with ZrO_2 or a highly dispersed CuO phase. In addition, the back shoulder, located at approximately 225 °C, could profile the reduction of isolated CuO species or large sizes of CuO [8,43,45–47]; however, we consider that the former reason plays a decisive role, based on the XRD results (Table 2). At the same time, a significantly broad reduction temperature range is displayed and implies unequal CuO particle size.

3.4. Catalytic activity of POM

Catalytic activity of the catalysts was tested through POM reaction and shown in Fig. 4. C_{MeOH} [Fig. 4 (a)] of catalysts display in an order of DP-CvZ-450 > CP-CvZ-450 > DP-CvZ-500 > DP-CvZ-550 > CZ > CZr at whole reaction temperature, but the F_{H_2} of DP-CvZ-500, and DP-CvZ-550 catalysts [Fig. 4 (b)] exhibited lower than that of CZ catalyst. Meanwhile, compared with the general catalyst (CZ), both DP-CvZ-450 and CP-CvZ-450 catalysts effectively promoted the catalytic activity, which performed almost ~99% of C_{MeOH}, ~95% of F_{H_2} at 250 °C, and also maintained ~70% of C_{MeOH} and >75% F_{H_2} at 150 °C. Hence, these oxygen vacancies may serve as the active sites for methanol and oxygen chemisorption. Another important judgment on catalytic activity over the catalysts for F_{CO} is displayed in Fig. 4 (c). The CZ, without oxygen vacancies, has higher F_{CO}, approximately 8% at 250 °C. At higher temperature (>200 °C), the F_{H_2} slightly decreases and F_{CO} increases due to reverse water gas shift (rWGS) reaction [48]. For DP-CvZ-450, it can reduce F_{CO} to 3.4% at 250 °C and even to 0% below 200 °C. Significantly, for both DP-CvZ-500 and DP-CvZ-550, F_{CO} reduces perfectly to 0% at whole reaction temperature. Meanwhile, the CP-CvZ-450 catalyst finds a lower F_{CO} than CZ, with F_{CO} only 5% at 250 °C and 2% at 150 °C being detected. Compared with our earlier study [21], which mentions CZ-based catalyst promoted by gold that has the advantage of not only decreasing CO selectivity, but also decreasing reaction temperature, both DP-CvZ-450 and CP-CvZ-450 catalysts without

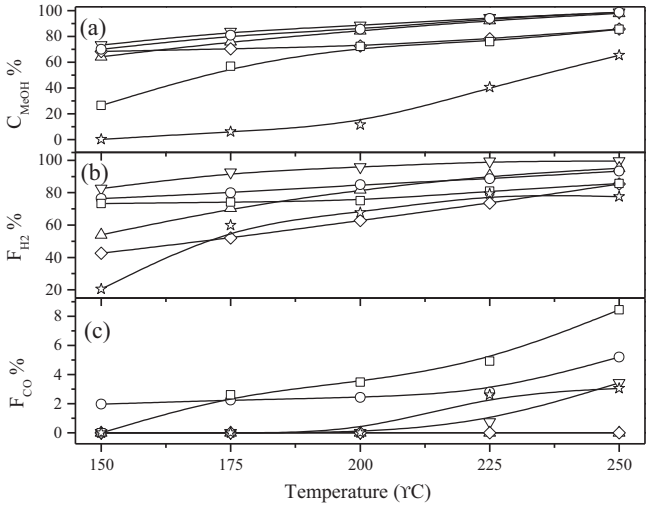

Fig. 4. (a) Methanol conversion, (b) Fraction of hydrogen in methanol being converted to H_2, and (c) Fraction of carbon in methanol being converted to CO plotted vs. reaction temperature during POM reaction over (▽) DP-CvZ-450, (△) DP-CvZ-500, (◊) DP-CvZ-550, (○) CP-CvZ-450, (□) CZ, and (☆) CZr catalysts.

any precious metal loading have similar efficiency, even much better.

Even so, the CZr catalyst has the worst performance (C_{MeOH} only 65% at 250 °C, and ~0% at 150 °C) due to the unequal size of CuO via TPR results. Possible reasons are that the variation in the chemical state of copper might modify charge properties or change the active crystallographic planes by ZrO_2 [11]. On the other hand, the ability of hydrogen spillover of ZrO_2 support is also worse than ZnO. Nevertheless, CZr catalyst also has good F_{CO} at only 3% (>200 °C) and 0% (<200 °C) due to oxygen vacancies on ZrO_2 (see Table 2).

Last but not least, catalytic stability is shown in Fig. 5, displaying an outstanding stability of DP-CvZ-450 catalyst, which maintains methanol conversion at around 75% after 72 h of continuous operation at 250 °C. This is better than the general CZ catalyst without oxygen vacancies on the surface (only about 65% remains after 72 h). At the same time, CZr catalyst has the worst methanol conversion (only around 55%), despite optimum stability. As the results show, we can further confirm that those oxygen vacancies could not only efficiently promote catalytic activity, but also raise catalytic stability. And speculation could be made that they could not only accelerate the reaction rate, but also simultaneously diminish the

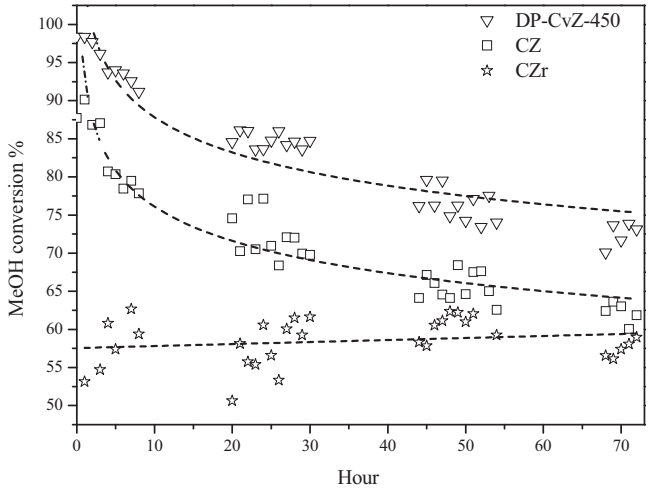

Fig. 5. Time-on-stream stability test of POM at 250 °C over (▽) DP-CvZ-450, (□) CZ, and (☆) CZr catalysts.

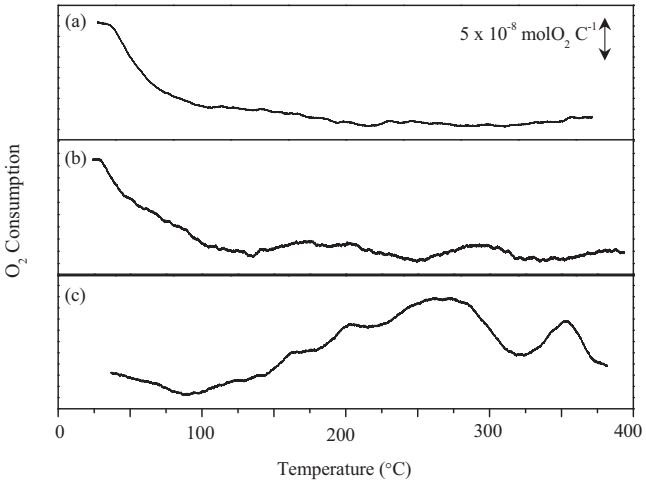

Fig. 6. The O_2-TPR profiles of freshly catalysts (a) Z, (b) vZ-450, and (c) vZ-500.

accumulation of heat which might let catalysts severely aggregate during the reaction.

3.5. The mechanism of CO oxidation on CvZ with oxygen vacancies

Although, the generation of CO evidently can be efficiently suppressed and even reach CO-free conditions on CvZ catalysts, the mechanism of CO oxidation on CvZ with oxygen vacancies should be discussed. In recent years, CO oxidation has been widely researched over precious metal catalysts, such as Au/ZrO_2, or Cu/CeO_2, etc. [49,50]. CeO_2 and ZrO_2 could play the major role of not only oxygen storage capacity, but also oxygen mobility via oxygen vacancies in the lattice [51,52]. It is believed that the oxygen vacancies are favored to adsorb oxygen to form superoxide (O_2^-) species, thereby catalyzing the CO oxidation reaction [53,54]. Consequently, in our case, we suggest that the catalysts with oxygen vacancies on the surface can promote the adsorption of reaction gases (oxygen and methanol) at lower temperature and generate moveable oxygen species while increasing CO oxidation. To confirm this mechanism, the O_2-TPD experiment was conducted on the ZnO samples, as shown in Fig. 6. The O_2-TPD profile of ZnO exhibits a desorption peak started from room temperature and decreased quickly at $T < 100\,^{\circ}C$ [Fig. 6 (a)]. This peak corresponds to the weak bonding of oxygen, which can easily desorb from the ZnO without oxygen vacancies. However, after modifying the surface properties, the desorption of O_2 is found not only at low temperature, but also at $T > 200\,^{\circ}C$ [Fig. 6 (b) and (c)]. Moreover, with increasing the amount of oxygen vacancies on the ZnO surface, the desorption of O_2 continued up to the end temperature of 450 °C. Comparing Fig. 6 (a) and (c), the amount of O_2 adsorbed on the surface of ZnO can be increased at least 70 times due to the existence of oxygen vacancies.

Furthermore, the in-situ DRIFTS of POM reaction gas chemisorptions on the catalyst w/wo oxygen vacancies at room temperature are discussed. Fig. 7 (I) shows that the gaseous MeOH band is located at the range of 3050–2800 cm^{-1} which can be assigned to the stretching of the C–H bond; however, it would shift to 2928, 2895, and 2814 cm^{-1}, contributed by methoxy groups (CH_3O^*) after being adsorbed on the catalyst [55,56]. Comparing the catalysts of Z and vZ-450, there are no adsorption peaks on Z catalyst, due to the lack of Cu species, which is the cardinal active site of methanol adsorption [55]. But the vZ-450 catalyst has obvious adsorption peaks which upon speculation suggest that the POM gases can be adsorbed onto the oxygen vacancy sites. Meanwhile, we can discover that the IR adsorption peaks of methoxy on DP-CvZ-450

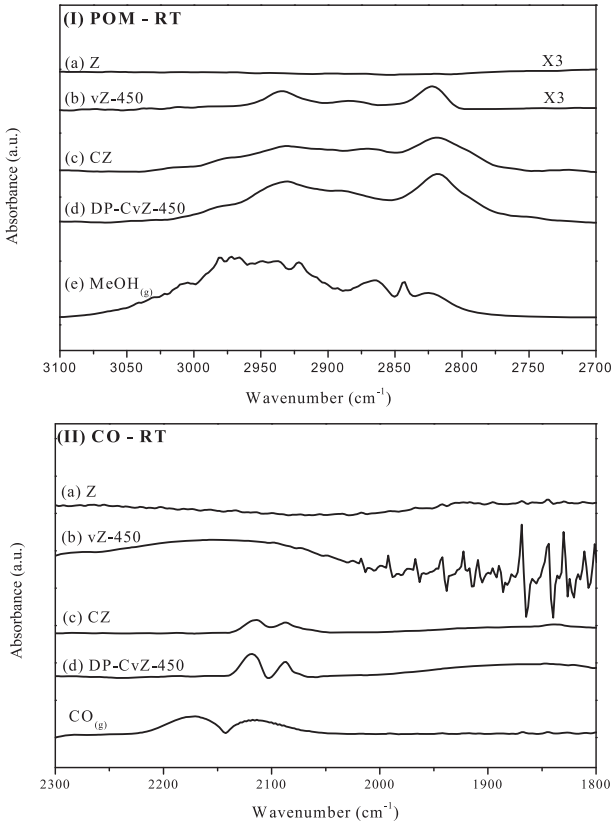

Fig. 7. In-situ DRIFTS for (I) POM reaction gases chemisorptions and (II) CO chemisorptions over (a) Z, (b) vZ-450, (c) CZ, and (d) DP-CvZ-450 catalysts.

catalyst are larger than on CZ catalyst, which means oxygen vacancies can effectively promote the POM gas chemisorption. To further confirm the effect of oxygen vacancies, another in-situ DRIFTS for CO chemisorption experiments is shown in Fig. 7 (II). The CO gas phase band is located at 2173 and 2115 cm^{-1}, and after CO chemisorption on the catalysts, the peaks shifted to 2082 and 2054 cm^{-1} [57]. It also obviously shows that more CO gases were adsorbed on the CvZ with oxygen vacancies. Significantly, oxygen vacancies provide sites for the adsorption of a particular gas containing oxygen atoms, such as oxygen, methanol, or carbon monoxide.

To further affirm whether the CO oxidation reaction is related to oxygen vacancies, the (I) 1st CO-TPR and (II) 2nd CO-TPR were tested and are shown in Fig. 8. Obviously, as shown in the 1st CO-TPR result [Fig. 8 (I)], the CuO reduction peak shifts from 240 to 165 °C when the catalyst contained oxygen vacancies. After the 1st CO-TPR, both catalysts w/wo oxygen vacancies were oxidized through air at room temperature for 0.5 h, and then the 2nd CO-TPR [Fig. 8 (II)] was done. Both catalysts w/wo oxygen vacancies have a broad peak at around 30–120 °C, which is the contribution of physical adsorption oxygen on the Cu surface. Regarding the catalyst containing oxygen vacancies, there also are other peaks at about 150 and 315 °C, which can be assigned to partial copper oxide on the surface and the oxidation of oxygen vacancies on ZnO surface, respectively. This result again indicates that oxygen vacancies may not only accelerate the rate of O_2 chemisorption and further oxidize surface Cu, which is an important initiation step in POM, but also accelerate CO chemisorption and catalytic reaction at low temperature (~150 °C).

Since the reactivity of POM is first dependent on chemisorbed methanol and oxygen, lower adsorbed temperature and higher concentration of these intermediates might be in response to the

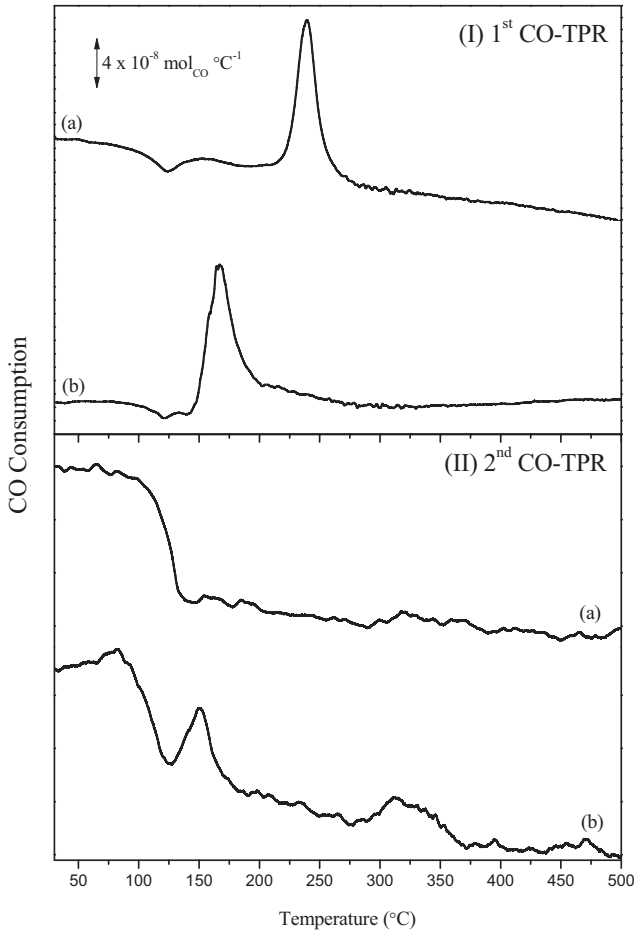

Fig. 8. (I) 1st CO-TPR and (II) 2nd CO-TPR of fresh (a) CZ and (b) DP-CvZ-450 catalysts.

existence of oxygen vacancies on the catalyst surface. When the reaction temperature exceeding the T_i (temperature start to produce hydrogen), those chemisorbed intermediates would quickly decompose and generate products, including H_2, CO_2, H_2O, and CO. To further realize the surface species or intermediates on the CZ and CvZ catalysts during the POM reaction, in-situ DRIFTS (Fig. 9) was examined. The IR spectra [Fig. 9 I (a) and (b)] of the surface species on the CZ catalyst in the POM reaction at 160 and 180 °C, display very weak absorbance bands of methoxy groups (CH_3O^*) at 2928, 2895, 2814, 1443, and 1060 cm^{-1} [55,56], and formate species at 2967, 2882, 1570, 1370 cm^{-1} [58], which were formed from the dehydrogenation of methoxy via formaldehyde [59]. By contrast, with the function of oxygen vacancies on the surface of CvZ-450 catalyst [Fig. 9 II (a) and (b)], more formate species were formed. Formaldehyde species is not detected in our present study which could be due to its rapid oxidation into formate species. Because oxygen is required for the partial oxidation of formaldehyde into dioxymethylene which is the precursor of formate, more moveable oxygen species existing on the surface of CvZ catalyst with oxygen vacancies [see TPD data in Fig. 6 (b) and (c)] might enhance the formation of formate. In addition, the bands at 1570 and 1370 cm^{-1} are specifically assigned to the asymmetric and symmetric O–C–O stretching of the adsorbed bidentate formate species, respectively [60,61]. It is interesting to find that more intensely symmetric O–C–O bidentate at 1360 cm^{-1} formate group formed on the CvZ catalyst at 160–180 °C [Fig. 9 II (a) and (b), III (a) and (b)], which should be due to bridging with the moveable oxygen on the metallic oxide. In addition, there was a broad band at 3100–3500 cm^{-1} which

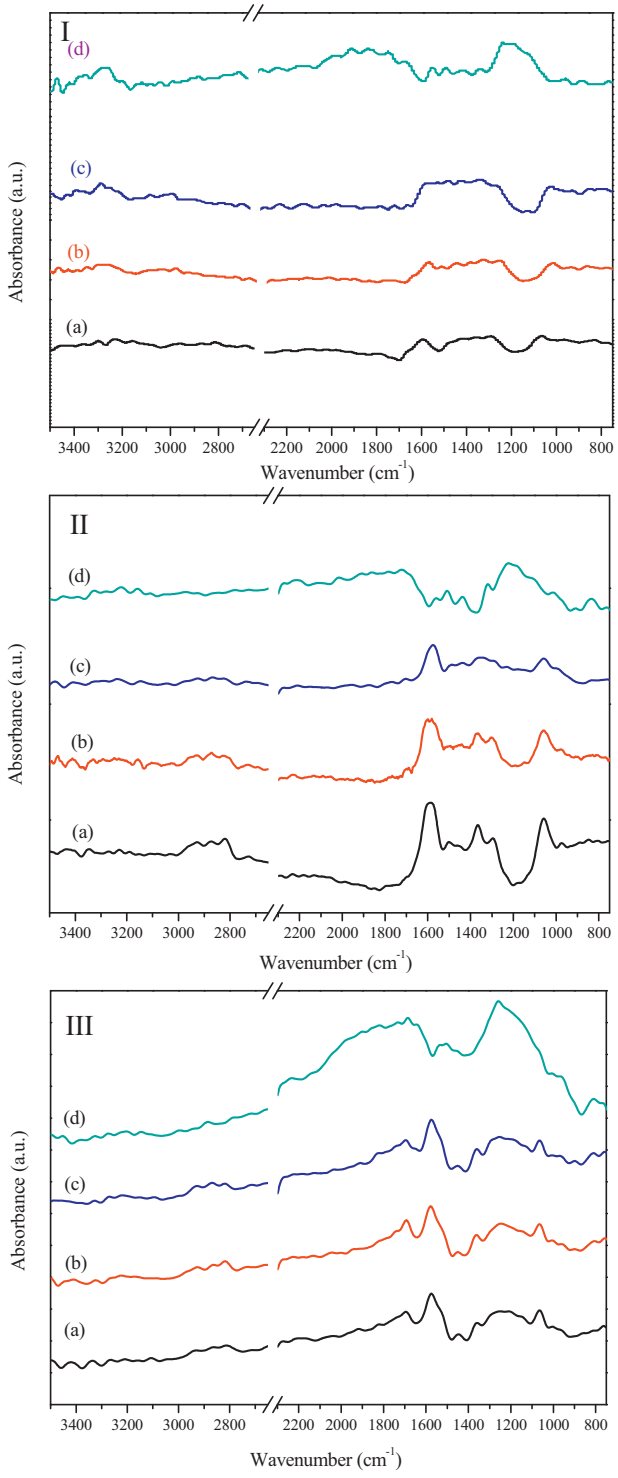

Fig. 9. In-situ DRIFTS spectra of surface species evolution during thermal treatment of methanol/oxygen adsorption on (I) CZ, (II) DP-CvZ-450, and (III) DP-CvZ-500 catalyst (a) 160 °C, (b) 180 °C, (c) 200 °C, and (d) 300 °C.

can be assigned to hydroxy groups (OH^*) increasing with temperature, implying that the oxygen source reacts with methanol to form OH^* groups on the CZ. However, comparatively weak absorbance peaks on the CvZ catalysts at $T > 200$ °C were observed. This implies moveable oxygen species on the surface of CvZ catalyst prefer not to combine with H^*, but more so with CO^*, or to form other carbonate species. Moreover, bidentate carbonate species at 1220 cm^{-1} were observed on the surface of CZ at

$T > 250\,^{\circ}C$ It usually formed on the surface of ZnO at high temperature due to the presence of Cu dissolved in the ZnO matrix which modified the support adsorption properties. Lack of oxygen vacancy on the surface of ZnO might restrict the movability of oxygen and result in the formation of surface carbonate. However, excess oxygen vacancies might provide more free moveable oxygen species on the ZnO surface and induce the formation of carbonate species. In evidence, carbonate species can be formed at 160 °C on the CvZ-500 and increase the amount with rising temperature [Fig. 9 III (a)–(d)]. Possible pathways are schemed as follows:

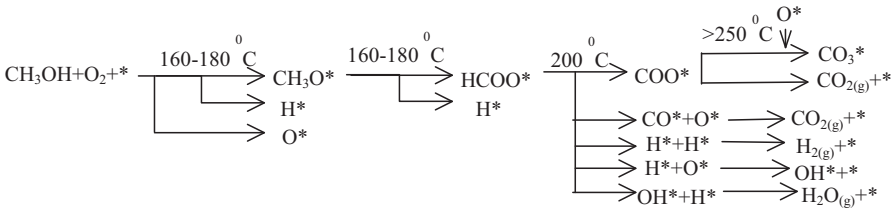

Moreover, according to Gibbs' free energy fundamental equations, the G° of CO oxidized reaction is −257.2 kJ/mol which is lower than the H_2O formation ($G^{\circ} = -228.6$ kJ/mol), so these moveable oxygen species would likely catalyze CO* to CO_2 first. Nevertheless, the H_2O formation would take place when overtaken by the amount of C_{ov} to completely catalyze CO.

Compared with our previous studies [21,29] concerning CuZn-based catalysts promoted by gold, the non-precious metallic CuZn catalysts containing oxygen vacancies can achieve analogous effects including lowering the POM reaction temperature (T_r), as well as improving catalytic reactivity, and lowering CO concentration much better.

4. Conclusions

We have successfully generated oxygen vacancies on non-precious metallic CuZn-based catalysts by simple and inexpensive preparation methods, including DP and CP. Furthermore, we also can fine tune the concentration of oxygen vacancies by adjusting calcination conditions, including atmosphere and temperature. The DP-CvZ-450 catalyst has the best catalytic activity, with almost complete conversion of methanol at 250 °C and maintaining good conversion around 75% at 150 °C. Higher hydrogen production and lower carbon monoxide (0–4%) also have been attained. Moreover, a CO-free situation (0%) at whole-reaction temperature can be achieved on the DP-CvZ-500 and DP-CvZ-550 which contained more oxygen vacancies, but extra C_{ov} might enhance the generation of H_2O and generate more carbonate species on the surface. In addition, our study supports the conclusion that oxygen atoms from POM gases (methanol and oxygen) would easily adsorb onto catalysts via oxygen vacancies and generate moveable oxygen species. The amount of O_2 adsorbed on the surface of ZnO can be increased at least 70 times due to the existence of oxygen vacancies. These oxygen vacancies efficiently assist with the decomposition or generation of intermediate species during the POM reaction, and simultaneously promote CO oxidation processes, as well as raise stability. Finally, without any other precious or transition metals, these catalysts can enormously reduce the cost, maintain high activity, and maybe open up new opportunities for other catalytic fields.

Acknowledgments

The authors are grateful for the financial support of this work by the National Science Council of Taiwan. We thank Professor Yun-Liang Soo (Department of Physics, National Tsing-Hua University) for help with the Raman spectroscopy experiments.

References

[1] Z.F. Wang, J.Y. Xi, W.P. Wang, G.X. Lu, J. Mol. Catal. A Chem. 191 (2003) 123–134.
[2] M.L. Cubeiro, J.L.G. Fierro, J. Catal. 179 (1998) 150–162.
[3] L.Y. Mo, X.M. Zheng, C.T. Yeh, Chem. Commun. (2004) 1426–1427.
[4] B.L. Kniep, T. Ressler, A. Rabis, F. Girgsdies, M. Baenitz, F. Steglich, R. Schlogl, Angew. Chem. Int. Ed. 43 (2004) 112–115.
[5] T. Ressler, B.L. Kniep, I. Kasatkin, R. Schlogl, Angew. Chem. Int. Ed. 44 (2005) 4704–4707.
[6] I. Kasatkin, P. Kurr, B. Kniep, A. Trunschke, R. Schlogl, Angew. Chem. Int. Ed. 46 (2007) 7324–7327.
[7] L.A. Espinosa, R.M. Lago, M.A. Pena, J.L.G. Fierro, Top. Catal. 22 (2003) 245–251.
[8] J. Agrell, H. Birgersson, M. Boutonnet, I. Melian-Cabrera, R.M. Navarro, J.L.G. Fierro, J. Catal. 219 (2003) 389–403.
[9] J. Agrell, M. Boutonnet, J.L.G. Fierro, Appl. Catal. A Gen. 253 (2003) 213–223.
[10] J. Agrell, M. Boutonnet, I. Melian-Cabrera, J.L.G. Fierro, Appl. Catal. A Gen. 253 (2003) 201–211.
[11] J. Agrell, K. Hasselbo, K. Jansson, S.G. Jaras, M. Boutonnet, Appl. Catal. A Gen. 211 (2001) 239–250.
[12] L. Alejo, R. Lago, M.A. Pena, J.L.G. Fierro, Appl. Catal. A Gen. 162 (1997) 281–297.
[13] Z.L. Wang, J.H. Song, Science 312 (2006) 242–246.
[14] J.H. Yang, X.Y. Liu, L.L. Yang, Y.X. Wang, Y.J. Zhang, J.H. Lang, M. Gao, M.B. Wei, J. Alloys Compd. 485 (2009) 743–746.
[15] S.D. Oosterhout, L.J.A. Koster, S.S. van Bavel, J. Loos, O. Stenzel, R. Thiedmann, V. Schmidt, B. Campo, T.J. Cleij, L. Lutzen, D. Vanderzande, M.M. Wienk, R.A.J. Janssen, Adv. Energy Mater. 1 (2011) 90–96.
[16] X.W. Wang, G. Liu, L.Z. Wang, Z.G. Chen, G.Q. Lu, H.M. Cheng, Adv. Energy Mater. 2 (2012) 42–46.
[17] S. Rawalekar, T. Mokari, Adv. Energy Mater. 3 (2013) 12–27.
[18] R. Levanmao, L. Dufresne, J.H. Yao, Appl. Catal. 65 (1990) 143–157.
[19] L. Chan, G.L. Griffin, Surf. Sci. 173 (1986) 160–175.
[20] L.Y. Mo, A.H. Wan, X.M. Zheng, C.T. Yeh, Catal. Today 148 (2009) 124–129.
[21] Y.J. Huang, K.L. Ng, H.Y. Huang, Int. J. Hydrogen Energy 36 (2011) 15203–15211.
[22] S.T. Liu, K. Takahashi, H. Eguchi, K. Uematsu, Catal. Today 129 (2007) 287–292.
[23] S.D. Jones, H.E. Hagelin-Weaver, Appl. Catal. B Environ. 90 (2009) 195–204.
[24] G. Huang, B.J. Liaw, C.J. Jhang, Y.Z. Chen, Appl. Catal. A Gen. 358 (2009) 7–12.
[25] S. Polarz, J. Strunk, V. Ischenko, M.W. van den Berg, O. Hinrichsen, M. Muhler, M. Driess, Angew. Chem. 45 (2006) 2965–2969.
[26] M. Kurtz, J. Strunk, O. Hinrichsen, M. Muhler, K. Fink, B. Meyer, C. Woll, Angew. Chem. Int. Ed. 44 (2005) 2790–2794.
[27] Y.G. Lin, Y.K. Hsu, S.Y. Chen, L.C. Chen, K.H. Chen, J. Mater. Chem. 20 (2010) 10611–10614.
[28] L.L. Yang, J.H. Yang, X.Y. Liu, Y.J. Zhang, Y.X. Wang, H.G. Fan, D.D. Wang, J.H. Lang, J. Alloys Compd. 463 (2008) 92–95.
[29] Y.J. Huang, K.L. Ng, H.Y. Huang, J. Chin. Inst. Eng. 34 (2011) 11–17.
[30] K. Vanheusden, W.L. Warren, C.H. Seager, D.R. Tallant, J.A. Voigt, B.E. Gnade, J. Appl. Phys. 79 (1996) 7983–7990.
[31] B.X. Lin, Z.X. Fu, Y.B. Jia, Appl. Phys. Lett. 79 (2001) 943–945.
[32] Q.X. Zhao, P. Klason, M. Willander, H.M. Zhong, W. Lu, J.H. Yang, Appl. Phys. Lett. 87 (2005) 211912-1–211912-3.
[33] Y. Dai, Y. Zhang, Y.Q. Bai, Z.L. Wang, Chem. Phys. Lett. 375 (2003) 96–101.
[34] A. Teke, U. Ozgur, S. Dogan, X. Gu, H. Morkoc, B. Nemeth, J. Nause, H.O. Everitt, Phys. Rev. B 70 (2004) 195207-1–195207-10.
[35] J.B.K. Law, J.T.L. Thong, Nanotechnology 19 (2008) 205502-1–205502-5 [artn 205502].
[36] B.J. Coppa, R.F. Davis, R.J. Nemanich, Appl. Phys. Lett. 82 (2003) 400–402.
[37] M. Ghosh, A.K. Raychaudhuri, Nanotechnology 19 (2008).
[38] A. Zubiaga, J.A. Garcia, F. Plazaola, F. Tuomisto, K. Saarinen, J. Zuniga Perez, V. Munoz-Sanjose, J. Appl. Phys. 99 (2006).
[39] N. Ashkenov, B.N. Mbenkum, C. Bundesmann, V. Riede, M. Lorenz, D. Spemann, E.M. Kaidashev, A. Kasic, M. Schubert, M. Grundmann, G. Wagner, H. Neumann, V. Darakchieva, H. Arwin, B. Monemar, J. Appl. Phys. 93 (2003) 126–133.
[40] G.H. Li, L.J. Hu, J.M. Hill, Appl. Catal. A Gen. 301 (2006) 16–24.
[41] W.C. Li, M. Comotti, F. Schuth, J. Catal. 237 (2006) 190–196.
[42] G. Fierro, M. LoJacono, M. Inversi, P. Porta, F. Cioci, R. Lavecchia, Appl. Catal. A Gen. 137 (1996) 327–348.
[43] L.C. Wang, Q. Liu, M. Chen, Y.M. Liu, Y. Cao, H.Y. He, K.N. Fan, J. Phys. Chem. C 111 (2007) 16549–16557.
[44] S.D. Jones, L.M. Neal, M.L. Everett, G.B. Hoflund, H.E. Hagelin-Weaver, Appl. Surf. Sci. 256 (2010) 7345–7353.
[45] D.Z. Zhang, H.B. Yin, C. Ge, J.J. Xue, T.S. Jiang, L.B. Yu, Y.T. Shen, J. Ind. Eng. Chem. 15 (2009) 537–543.
[46] B. Lindstrom, L.J. Pettersson, P.G. Menon, Appl. Catal. A Gen. 234 (2002) 111–125.
[47] J. Sloczynski, R. Grabowski, A. Kozlowska, P.K. Olszewski, J. Stoch, Phys. Chem. Chem. Phys. 5 (2003) 4631–4640.
[48] S. Velu, K. Suzuki, M. Okazaki, M.P. Kapoor, T. Osaki, F. Ohashi, J. Catal. 194 (2000) 373–384.
[49] A. Wolf, F. Schuth, Appl. Catal. A Gen. 226 (2002) 1–13.
[50] W. Liu, M. Flytzani-Stephanopoulos, J. Catal. 153 (1995) 304–316.
[51] W. Liu, M. Flytzani-Stephanopoulos, J. Catal. 153 (1995) 317–332.
[52] G.J.J. Bartley, R. Burch, Appl. Catal. 43 (1988) 141–153.
[53] C. Bozo, N. Guilhaume, J.M. Herrmann, J. Catal. 203 (2001) 393–406.
[54] Z.Y. Pu, X.S. Liu, A.P. Jia, Y.L. Xie, J.Q. Lu, M.F. Luo, J. Phys. Chem. C 112 (2008) 15045–15051.
[55] G.J. Millar, C.H. Rochester, K.C. Waugh, J. Chem. Soc. Faraday Trans. 88 (1992) 2257–2261.
[56] J.P. Camplin, E.M. McCash, Surf. Sci. 360 (1996) 229–241.
[57] X.L. Zhu, Y.B. Xie, C.J. Liu, Y.P. Zhang, J. Mol. Catal. A Chem. 282 (2008) 67–73.
[58] D. Bianchi, T. Chafik, M. Khalfallah, S.J. Teichner, Appl. Catal. A Gen. 123 (1995) 89–110.
[59] C. Barnes, P. Pudney, Q.M. Guo, M. Bowker, J. Chem. Soc. Faraday Trans. 86 (1990) 2693–2699.
[60] S.T. Yong, K. Hidajat, S. Kawi, Catal. Today 131 (2008) 188–196.
[61] E. Finocchio, G. Busca, Catal. Today 70 (2001) 213–225.